arXiv:1605.03114v4 [cond-mat.mes-hall] 21 Nov 2016

Selective coherent phonon mode generation in single wall carbon nanotubes

Ahmad. R. T. Nugraha, Eddwi H. Hasdeo, and Riichiro Saito

Department of Physics, Tohoku University, Sendai 980-8578, Japan

E-mail: nugraha@flex.phys.tohoku.ac.jp

Abstract. The pulse-train technique within ultrafast pump-probe spectroscopy is theoretically investigated to excite a specific coherent phonon mode while suppressing the other phonon modes generated in single wall carbon nanotubes (SWNTs). In particular, we focus on the selectivity of the radial breathing mode (RBM) and the G-band for a given SWNT. We find that if the repetition period of the pulse train matches with integer multiple of the RBM phonon period, the RBM amplitude could be kept while the amplitudes of the other modes are suppressed. As for the G-band, when we apply a repetition rate of half-integer multiple of the RBM period, the RBM could be suppressed because of destructive interference, while the G-band still survives. It is also possible to keep the G-band and suppress the RBM by applying a repetition rate that matches with integer multiple of the G-band phonon period. However, in this case we have to use a large number of laser pulses having a property of "magic ratio" of the G-band and RBM periods.

PACS numbers: 78.67.Ch,63.22.-m,73.22.-f,78.67.-n

1. Introduction

Ultrashort laser pulses that are given to a single wall carbon nanotube (SWNT) sample with duration less than a phonon period in the SWNT may generate lattice oscillations coherently, which is usually called as the coherent phonons [1–5]. Quantum mechanically, these oscillations can be treated using the concept of coherent states, in which the amplitude-phase uncertainty reach its minimum value [6–9]. Recently, by using sub-10-fs laser pulses, more than 10 coherent phonon modes with frequency around 100–3000 cm^{-1} could be observed in a (6,5) enriched single-chirality SWNT sample [10]. This finding opened up possibilities to utilize a particular coherent phonon mode of the SWNT with a wide frequency range in the THz regime for nanomechanics applications, such as high-Q resonators [11], as well as quantum information science [12, 13]. However, we have to select a single coherent phonon mode with a well-defined frequency and suppress other phonon modes that have been excited, which is not possible to achieve by using only a single pulse of laser.

One possible technique to selectively excite a particular phonon mode is by using multiple pulses with a determined repetition rate in pump-probe spectroscopy. Since two decades ago, several experimental studies have used femtosecond pulse sequences for optical manipulation of molecular motion [14], for enhancement of optical phonons in mixed crystals [15], and also for controlling lattice dynamics at metal surfaces [16]. In the case of SWNTs, Kim *et al.* have recently shown that, by introducing pulse shaping [17], multiple pulses with the different repetition rates that are matched to some radial breathing mode (RBM) frequencies (around 5.5–7.5 THz) can be used to excite the RBMs of specific SWNTs in a bundled SWNT sample. The bundled SWNT sample consists of several tube species having different chiralities, represented by a set of integers (n, m), which give the SWNT circumferencial lengths and diameters [18]. Since the RBM frequency is inversely proportional to the SWNT diameter [19], different RBM frequencies will be excited at the same time if we only use a single laser pulse without pulse shaping. By applying the pulse train with a frequency matching to a RBM frequency of a single chirality SWNT, it is possible to excite the RBM of the specified SWNT in the bundled sample [17].

To our knowledge, it has not been shown yet whether or not the pulse-train technique can be used to generally excite a specific coherent phonon mode other than the RBMs in SWNTs, for example, the G-bands in the SWNTs, which have higher frequency (∼47.7 THz). Moreover, it is also interesting to investigate whether or not we can selectively generate a particular coherent phonon mode for a single-chirality SWNT which is mixed in the bundled sample. Due to the classical nature of coherent phonon oscillations [6], either in an enriched single-chirality sample or mixed bundled sample, one might think that it is trivial to selectively excite a specific phonon mode just by using a pulse train repetition frequency which is matched to the phonon frequency. However, we will show in this paper that, based on both numerical and analytical methods, the frequency matching is not the only condition to obtain the selective coherent phonon generation. Further considerations such as the dependence of phonon selectivity on the number of pulses and on frequency ratio of different phonon modes are also discussed.

This paper is organized as follows. In section 2.1, we overview the way to calculate the coherent phonon amplitudes and spectra. We basically follow the methods described in our previous papers [20, 21], which now takes into account several laser pulses in the pulse train. Besides the numerical method, we also show a possible description for the selective phonon excitation from the analytical solution of a driven force oscillator, which is given in section 2.2. In sections 3, particularly in 3.1 and 3.2, we discuss how we can selectively excite the radial breathing mode (RBM) and the G-band for a given SWNT by considering some adjustable external parameters such as the laser pulse width and the pulse repetition rate (or repetition period). We examine some conditions in which each of the phonon modes can be either kept surviving or suppressed. In 3.3, we briefly discuss the results the effects of carrier relaxation on coherent phonon generation. Conclusion and perspective are given in section 4.

2. Methods

2.1. Numerical simulation

We define a coherent phonon mode with wavevector $q = 0$ (Γ point phonon) whose amplitude Q_m satisfies

a driven oscillator equation [7–9]

$$\frac{\partial^2 Q_m(t)}{\partial t^2} + \omega_m^2 Q_m(t) = S_m(t), \tag{1}$$

where m labels the phonon mode and ω_m is the phonon frequency. Equation (1) is solved subject to the initial conditions $Q_m(0) = 0$ and $\dot{Q}_m(0) = 0$. The driving force $S_m(t)$ in the right hand side of equation (1) is given by

$$S_m(t) = -\frac{2\omega_m}{\hbar} \sum_{nk} \mathcal{M}_n^m(k) \left[f_n(k,t) - f_n^0(k) \right], \tag{2}$$

where $f_n(k,t)$ is the time-dependent electron distribution function and $f_n^0(k)$ is the initial equilibrium electron distribution function before pump pulse is applied. The derivation and justification of equations (1) and (2) is provided, for example, in reference [7]. Here n labels an electronic state, while k gives the electron wavevector. The electronic states of a SWNT are calculated within the extended tight-binding (ETB) approximation [22]. The electron-phonon matrix element $\mathcal{M}_n^m(k)$ is a simplified notation for $\mathcal{M}_{nk;nk}^{m,0}$, where $\mathcal{M}_{n'k';nk}^{m,q}$ is the electron-phonon matrix element in the ETB model with phonon wavevector $q = k - k'$ and with a transition from an electronic band n to n' [23]. It should be noted that in equation 1, we neglect the phonon damping term which originates from the anharmonicity [21]. We expect that if the phonon damping is included, an additional damping term modifying the coherent phonon amplitude will appear due to the dephasing time of the coherent phonon, which could then modulate the coherent phonon amplitude. However, looking at some experimental measurements on the phonon dephasing in SWNTs by single pulse pump-probe spectroscopy we estimate that even the G-band, which has a high frequency, can survive up to 5 ps [24]. Therefore, we expect that the phonon damping is not a key factor contributing to the selective phonon excitation.

In ultrafast pump-probe spectroscopy, a pump laser pulse should have much shorter pulse width (∼10 fs) compared with a typical coherent phonon period (∼ 20–100 fs). The observed coherent phonon intensity is proportional to the power spectrum of the oscillations of optical properties [6]. We see in equation 2 that the driving force $S_m(t)$ depends on the photoexcited electron distribution functions, which can be calculated by considering the photogeneration of electrons. The photogeneration rate from Fermi's golden rule is obtained as [25]:

$$\begin{aligned}\frac{\partial f_n(k,t)}{\partial t} = {} & \frac{8\pi^2 e^2\ u(t)}{\hbar\ n_g^2\ (E_{\rm pump})^2} \left(\frac{\hbar^2}{m_0}\right) \sum_{n'} |P_{nn'}(k,t)|^2 \\ & \times \Big(f_{n'}(k,t) - f_n(k,t) \Big) \\ & \times \delta\Big(E_{nn'}(k,t) - E_{\rm pump} \Big),\end{aligned} \tag{3}$$

where $E_{nn'}(k,t) = |E_n(k,t) - E_{n'}(k,t)|$ are the k dependent transition energies for a given SWNT at time t of phonon oscillation, $E_{\rm pump}$ is the pump laser energy, $P_{nn'}(k,t)$ is the optical matrix element obtained within the dipole approximation [22,26], and $u(t)$ is the time-dependent energy density of the pump pulse. It should be noted that $E_{nn'}(k,t)$ and $P_{nn'}(k,t)$ are modulated by $Q_m(t)$ of equation (1) through the change of the C–C bond length [17,27].

The energy density of pump pulse, $u(t)$, is related with the pump fluence F by a relation $F = (c/n_g)\int u(t)dt$, in which $u(t)$ is also assumed to be a Gaussian. We define a single Gaussian pulse with an index j as

$$u_j(t) = A_p e^{-4(t-t_j)^2 \ln 2/2\tau_p^2}, \tag{4}$$

where $A_p = (2n_g F\sqrt{\ln 2/\pi})/(c\tau_p)$, with c is the speed of light, τ_p is the laser pulse width, and t_j is the time at which the peak of the Gaussian is located. We set the fluence $F = 10^{-5}$ J cm^{-2} and refractive index $n_g = 1$. For the multiple Gaussian pulses constituting the pulse train, we can sum up several $u_j(t)$ as follows:

$$\begin{aligned} u(t) &= \frac{1}{N_p} \sum_{j=0}^{N_{\rm pulse}-1} u_j(t) \\ &= \frac{1}{N_p} \sum_{j=0}^{N_{\rm pulse}-1} A_p e^{-4(t-t_j)^2 \ln 2/2\tau_p^2}, \end{aligned} \tag{5}$$

where $N_{\rm pulse}$ is the number of pulses and t_j can be expressed as $t_j = jT_{\rm rep}$ with $T_{\rm rep}$ is the pulse repetition period, defined by the time interval between two neighboring Gaussian pulses. The normalization constant, N_p, appearing in equation 5 is taken into account when we assume that the pulse train is created by dividing a single laser pulse into $N_{\rm pulse}$. In the simplest case, $N_p = N_{\rm pulse}$, i.e., the source laser pulse is equally divided into $N_{\rm pulse}$ Gaussians. However, if we consider another pulse shaping, we generally have to integrate the pulse train laser density so that it has the same laser fluence as the source laser pulse.

We can also consider carrier relaxation or decay process in addition to the photogeneration process. Some experimental works have reported that the photoexcited electrons and holes in SWNTs are nonradiatively recombined via multiphonon emission processes within 1 ps time scale, which is one order of magnitude slower than in graphite [28, 29]. We can take these effects into account by adding a phenomenological term to the photogeneration rate in equation (3) as follows:

$$\left[\frac{\partial f_n(k,t)}{\partial t}\right]_r = -\frac{1}{\tau_r}[f_n(k,t) - f_n^0(k)], \tag{6}$$

where τ_r is the phenomenological relaxation time. When it is necessary to consider the carrier relaxation

effects, we can add the relaxation term of the form of equation (6) to the photogeneration rate in equation (3) and solve them as a whole.

In coherent phonon spectroscopy, a probe pulse is used to measure the absorption coefficient of the SWNT, $\alpha(t)$, at a probe energy E_{probe} and time t:

$$\alpha(E_{\text{probe}},t) \propto \sum_{nn'} \int dk |P_{nn'}(k,t)|^2 \left[f_n(k,t) - f_{n'}(k,t)\right] \times \delta\left[E_{nn'}(k,t) - E_{\text{probe}}\right]. \quad (7)$$

In this process, excitation of coherent phonons by the laser pump affects the optical properties of the SWNTs, which gives rise to the modulation of absorption coefficient $\Delta\alpha$. It should be noted that, in the numerical calculation, the delta functions in equations (3) and (7) are approximated by a Lorentzian line shape. The expression of $\Delta\alpha$ is given by

$$\Delta\alpha(E_{\text{probe}},t) = -[\alpha(E_{\text{probe}},t) - \alpha(E_{\text{probe}},-\infty)], \quad (8)$$

where $t = -\infty$ corresponds to the absence of pump pulse. The coherent phonon signal is represented by intensity I, which corresponds to the Fourier power spectrum of $\Delta\alpha$ at a given energy E_{probe}:

$$I(\omega) = \int e^{-i\omega t} \left|\Delta\alpha(E_{\text{probe}},t)\right|^2 dt, \quad (9)$$

where ω denotes the phonon frequency contributing to the coherent phonon spectra.

2.2. Analytical solution

By some approximations, it is possible to derive an analytical solution to the driven force oscillator considering the pulse train. Firstly, we start with equation (1) using the following simplified notation,

$$\frac{\partial^2 Q(t)}{\partial t^2} + \omega_0^2 Q(t) = S(t), \quad (10)$$

where ω_0 is the phonon frequency, and here we have omitted the index m from equation (1). We can solve equation (10) by using Green's function method which results in the following integration problem:

$$Q(t) = \int d\omega \int dt' \frac{1}{\omega_0^2 - \omega^2} e^{i\omega(t-t')} S(t') dt'. \quad (11)$$

Determining the shape of $S(t)$ is now important to explain the phenomena of coherent phonon oscillations. It has been known from earlier studies that coherent phonon oscillations may be driven by a displacive force or impulsive force, where the basic shape of the driving force is close to a step function or delta function, respectively [6, 9]. In the case of SWNTs, the driving force from photoexcited carriers interacting with SWNT lattices has been proposed to be displacive, i.e., the shape is close to a step function with a broadening factor determined by the laser pulse width τ_p [27]. When we consider the pulse train, we thus expect that the driving force will be like a staircase, where there are some steps originating from the number of pulses N_{pulse}. It is noted that solving the driven oscillator problem by combining τ_p and N_{pulse} for the staircase function is numerically feasible. However, an exact analytical solution is quite complicated to obtain. In this case, we assume that τ_p can be omitted from the driving force for simplicity. On the other hand, for the impulsive driving force, we may approximate the shape of the driving force by Gaussian function. where it is possible to obtain an exact analytical solution for $Q(t)$ even by combining τ_p and N_{pulse} in the driving force. In this section, we derive analytical $Q(t)$ solutions for both cases. We will show later in the discussion section that the two solutions can be equivalent when we focus on the maximum amplitudes of the oscillations, which implies that the presence of the pulse train with N_{pulse} does not care on the type of the force, whether it is displacive or impulsive.

For the displacive force, we assume the following form of the individual driving force component,

$$S_D(t') = A_D \Theta(t' - t_j) e^{-\gamma_r t'}, \quad (12)$$

where A_D is the displacive driving force amplitude, $\gamma_r = 1/\tau_r$ is the relaxation rate parameter, and $\Theta(t' - t_j)$ is the Heaviside step function with nonzero values (equal to unity) starting from t_j. By inserting equation (12) into (11) and using the residue theorem, the $Q(t)$ solution for one pulse of the displacive force is obtained as

$$Q_D(t) = 2\pi A_D \left[\frac{e^{-\gamma_r t_j}}{\omega_0(\gamma_r^2 + \omega_0^2)}\Big(\gamma_r \sin\omega_0(t - t_j) - \omega_0 \cos\omega_0(t - t_j)\Big) + \frac{e^{-\gamma_r t}}{\gamma_r^2 + \omega_0^2}\right]. \quad (13)$$

The full $Q_D(t)$ solution considering N_{pulse} with substituting $\omega_0 = 2\pi/T_0$ and $t_j = jT_{\text{rep}}$ is given by

$$Q_D(t) = 2\pi A_D \sum_{j=0}^{N_{\text{pulse}}-1} \left[\frac{T_0 e^{-\gamma_r j T_{\text{rep}}}}{2\pi(\gamma_r^2 + (\frac{2\pi}{T_0})^2)}\Big\{\gamma_r \sin\big(\frac{2\pi}{T_0}(t - jT_{\text{rep}})\big) - \frac{2\pi}{T_0}\cos\big(\frac{2\pi}{T_0}(t - jT_{\text{rep}})\big)\Big\} + \frac{e^{-\gamma_r t}}{\gamma_r^2 + (\frac{2\pi}{T_0})^2}\right], \quad (14)$$

where T_0 is the phonon period of a particular mode.

For the impulsive force, we assume that $S(t')$ in equation (11) can be represented by the Gaussian function with a peak at t_j and pulse width τ_p. The individual impulsive driving force can be written as

$$S_I(t') = A_I e^{-(t'-t_j)^2/\tau_p^2} e^{-\gamma_r t'}, \quad (15)$$

where A_I is the impulsive driving force amplitude. Inserting equation (15) into (11) and solving the

differential equation, $Q(t)$ for one pulse of this impulsive force is obtained as

$$Q_I(t) = \frac{2A_I\pi^{3/2}\tau_p}{\omega_0} e^{-[\gamma_r t_j + (\omega_0^2-\gamma_r^2)\tau_p^2/4]} \times \sin[\omega_0(t - t_j + \gamma_r\tau_p^2/2)]. \quad (16)$$

For $N_{\rm pulse}$ Gaussians, and also substituting $\omega_0 = 2\pi/T_0$ and $t_j = jT_{\rm rep}$, we obtain

$$Q_I(t) = A_I\sqrt{\pi}\tau_p T_0 \sum_{j=0}^{N_{\rm pulse}-1} e^{-[\gamma_r jT_{\rm rep} + ((2\pi/T_0)^2-\gamma_r^2)\tau_p^2/4]} \times \sin\left[\frac{2\pi}{T_0}(t - jT_{\rm rep} + \gamma_r\tau_p^2/2)\right], \quad (17)$$

We will use equations (14) and (17) to analyze numerical results in the next section.

3. Results and discussion

In the following calculations, we focus to discuss the results for a $(11,0)$ SWNT. This chirality is chosen in this work due to its less expensive calculation cost compared with other chiralities having a larger number of atoms in the unit cell. Yet, the $(11,0)$ SWNT is quite representative for understanding more general results. We set a certain laser energy $E_{\rm pump} = E_{\rm probe} = 1.75\,$eV, which is near the second optical transition energy E_{22} of the $(11,0)$ SWNT. The light polarization is fixed parallel to the SWNT axis. The RBM phonon period ($T_{\rm RBM}$) for the $(11,0)$ SWNT is about 111.5 fs, while the G-band period ($T_{\rm G}$) is about 20.9 fs. We firstly neglect the the carrier relaxation effects ($\gamma_r = 0$) in the discussions in sections 3.1 and 3.2 for simplicity. Then, we discuss the results including the relaxation effects in section 3.3 to understand what properties will be affected by the carrier relaxation.

3.1. RBM selective excitation

In figure 1, we show the calculated results for the RBM mode selection in the $(11,0)$ SWNT. Figure 1(a) shows the pulse train consisting of six Gaussian pulses ($N_{\rm pulse} = 6$) for several different repetition periods $T_{\rm rep}$. The repetition period $T_{\rm rep}$ in figure 1 is expressed as a multiple of the RBM phonon period, $T_{\rm RBM}$. For each pulse train, we use $\tau_p = 50\,$fs so that the coherent G-band ($T_{\rm G} = 20.9\,$fs) would not be excited. Example driving forces $S(t)$ due to laser pulse trains in figure 1(a) are given in figure 1(b), in which we show the case of $T_{\rm rep} = T_{\rm RBM}$ and $T_{\rm rep} = 1.5\ T_{\rm RBM}$, and we also display the driving force in the case of a single pulse (i.e., not a pulse train) for comparison. The driving forces are of displacive type based on the concept of electron-phonon and electron-photon interactions developed in section 2.1. Figure 1(c) shows the resulting coherent RBM phonon amplitudes excited

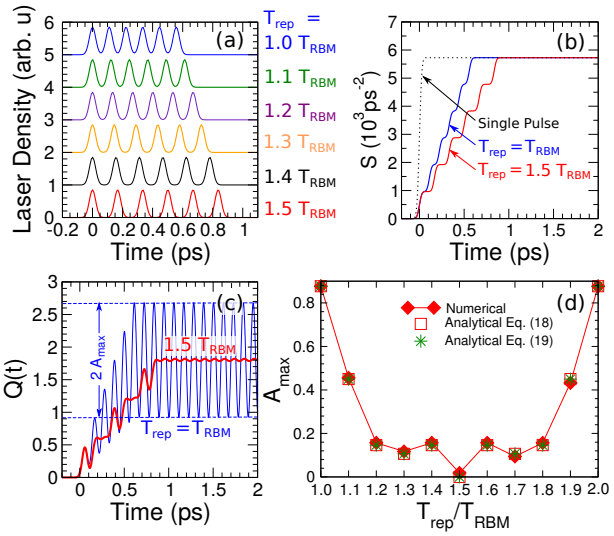

Figure 1. (a) Laser energy density $u(t)$ for several different pulse train repetition periods $T_{\rm rep}$ (1.0–1.5 $T_{\rm RBM}$) which are used to generate the RBM in an $(11,0)$ SWNT. Here $N_{\rm pulse} = 6$ and $T_{\rm RBM}$ for the $(11,0)$ SWNT is about 111.5 fs. For each pulse train, we consider $\tau_p = 50\,$fs. (b) The driving force $S(t)$ due to laser pulse trains in (a), shown only for the case of $T_{\rm rep} = T_{\rm RBM}$ and $T_{\rm rep} = 1.5\ T_{\rm RBM}$. The driving force in the case of a single pulse (not pulse train) is given in dotted line for comparison. (c) The resulting coherent phonon amplitudes $Q(t)$ generated by $S(t)$ in (b), shown for the case of $T_{\rm rep} = T_{\rm RBM}$ and $T_{\rm rep} = 1.5\ T_{\rm RBM}$. We additionally define a maximum amplitude $A_{\rm max}$, which is shown in panel (c) for $T_{\rm rep} = T_{\rm RBM}$ as an example. (d) The maximum amplitude for each $Q(t)$ as a function of pulse train repetition period. Filled diamonds are from the numerical calculation, while open squares and stars are from two different analytical approaches. The analytical $A_{\rm max}$ values are normalized to the numerical value of $A_{\rm max}$ at $T_{\rm rep} = T_{\rm RBM}$.

by the driving forces from figure 1(b) for $T_{\rm rep} = T_{\rm RBM}$ and $T_{\rm rep} = 1.5\ T_{\rm RBM}$. To check further behavior of the coherent phonon oscillation by changing the pulse repetition period, we define $A_{\rm max}$ in figure 1(c) as the maximum amplitude of the oscillation. In figure 1(d), we show $A_{\rm max}$ for several $T_{\rm rep}$ values within 1.0–2.0 $T_{\rm RBM}$.

From figure 1(d), we can see that the numerical value of $A_{\rm max}$ in the case of $N_{\rm pulse} = 6$ is the largest (smallest) for $T_{\rm rep} = T_{\rm RBM}$ ($T_{\rm rep} = 1.5\ T_{\rm RBM}$). This numerical result can be reproduced analytically using both equations (14) and (17) considering $\gamma_r = 0$ and $T_0 = T_{\rm RBM}$. We firstly simplify equation (14) so that it reduces to

$$Q_D(t) \propto \sum_{j=0}^{N_{\rm pulse}-1} \left\{1 + \cos\left[2\pi\left(\frac{t - jT_{\rm rep}}{T_0}\right)\right]\right\}, \quad (18)$$

while equation (17) reduces to

$$Q_I(t) \propto \sum_{j=0}^{N_{\rm pulse}-1} e^{-\pi^2\left(\frac{\tau_p}{T_0}\right)^2} \sin\left[2\pi\left(\frac{t - jT_{\rm rep}}{T_0}\right)\right], \quad (19)$$

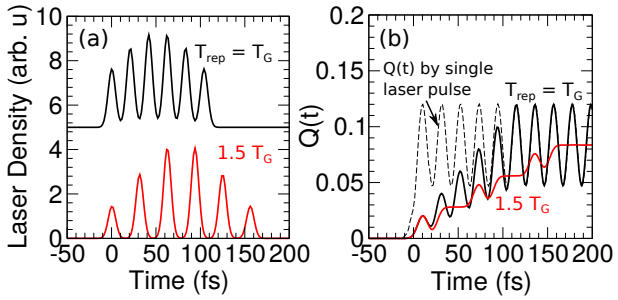

Figure 2. Selection of the G-band of the (11,0) SWNT by a pulse train with $T_{\rm rep}$ varied in terms of $T_{\rm G}$. We excite the coherent phonons by laser pulses with $\tau_p = 10\,$fs and $N_{\rm pulse} = 6$. Panel (a) shows the laser density of the pulse train with $T_{\rm rep} = T_{\rm G}$ and $T_{\rm rep} = 1.5\ T_{\rm G}$, while panel (b) shows the resulting coherent G-band phonon amplitude. For additional comparison, we show a dashed line that represents the G-band amplitude generated by a single laser pulse.

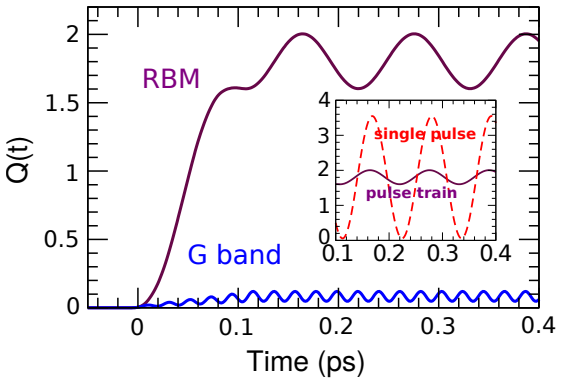

Figure 3. The coherent RBM and G-band phonon amplitudes for the (11,0) SWNT excited by the same pulse train consisting of six Gaussian pulses with $\tau_p = 10\,$fs and $T_{\rm rep} = T_{\rm G} = 20.9\,$fs. Inset shows comparison between the RBM phonon excited by a single Gaussian pulse (dashed line) and that by the pulse train with $N_{\rm pulse} = 6$ (solid line) taken from the main figure.

To compare the analytical solution with the numerical result on the same plot, we calculate the analytical $A_{\rm max}$ values for different $T_{\rm rep}$ from equations (18) and (19) normalized to numerical $A_{\rm max}$ at $T_{\rm rep} = T_0 = T_{\rm RBM}$. As shown in Fig. 1(d), the agreement between the analytical and numerical results is quite excellent. In fact, if we perform the summations in equations (18) and (19) explicitly to calculate $A_{\rm max}$ as defined in figure 1(c), we find that both equations will have the same form of $A_{\rm max}$ as follows:

$$A_{\rm max} \propto \left| \frac{\sin[N_{\rm pulse}\pi(T_{\rm rep}/T_0)]}{\sin[\pi(T_{\rm rep}/T_0)]} \right|. \qquad (20)$$

Equation (20) suggests that by using the pulse-train technique, the behavior of $A_{\rm max}$ is independent of the detailed shape of the constituting force. From both numerical and analytical results, we can also see that the value of $A_{\rm max}$ at $T_{\rm rep} = T_{\rm RBM}$ is recovered at $T_{\rm rep} = 2T_{\rm RBM}$, which is also expected for higher integer-multiple of $T_{\rm RBM}$. It indicates that as long as the pulse repetition period matches integer multiple (half-integer multiple) of the RBM period, we will mostly have the coherent RBM phonon amplitude enhanced (suppressed). It should be noted from equation (20) that the shape of $A_{\rm max}$ as a function of $T_{\rm rep}/T_{\rm RBM}$ is also $N_{\rm pulse}$-dependent. In particular, if $N_{\rm pulse}$ is an even (odd) number, $A_{\rm max}$ is zero (nonzero but small) at $T_{\rm rep}$ equals half-integer multiple of $T_{\rm RBM}$.

3.2. G-band selective excitation

In figure 2, we present a similar calculation for the G-band phonon mode, which has a higher-frequency (shorter period) than the RBM. In this case, $T_{\rm G}$ for the $(11, 0)$ SWNT is about 20.9 fs. Morover, to consider an experimental condition in which a Gaussian pulse shaping (or an envelope function for multiple pulses) is used to obtain a narrow spectral shape [17], we multiply $u(t)$ with a Gaussian function having a width of half of the total pulse duration. We then normalize the new $u(t)$ so as the pump fluence F is the same as in the case of using a single Gaussian pulse. Figure 2(a) shows the pulse train profile consisting of six Gaussian pulses with the pulse width $\tau_p = 10\,$fs. The pulse train in figure 2(a) is varied with two different repetition periods: $T_{\rm rep} = T_{\rm G}$ and $T_{\rm rep} = 1.5\ T_{\rm G}$. In figure 2(b), we show the resulting coherent phonon amplitude by the two cases of pulse train, which is also compared with the amplitude excited by a single Gaussian pulse. It can be seen that the pulse repetition period which matches to the integer multiple (half-integer multiple) of the G-band period will mostly enhance (suppress) the G-band phonon amplitude. However, we find that actually for the higher-frequency coherent phonon modes such like the G-band (which has smaller amplitudes than the RBM), the repetition rate with the value of the integer multiple of the G-band period is *not always* sufficient to completely suppress the RBM amplitude although the G-band amplitude is already at its possible largest value.

In figure 3, we show a comparison between the coherent RBM and G-band phonon amplitudes excited with $\tau_p = 10\,$fs and $T_{\rm rep} = T_{\rm G} = 20.9\,$fs laser pulses. We can see that the RBM still has a larger amplitude compared with the G-band excited by the same pulse train. We expect that the origin of this behavior is due to the dependence of the phonon amplitude on the phonon frequency, in which $Q_m(t)$ is inversely proportional to ω_m upon solving the equation (1), i.e., the higher-frequency phonon modes tend to have a smaller amplitude than the lower frequency modes [27], as is also indicated by equations (13) and (16). We note that the choice of $T_{\rm rep} = T_{\rm G}$ for the case shown in figure 3 still does not completely give a

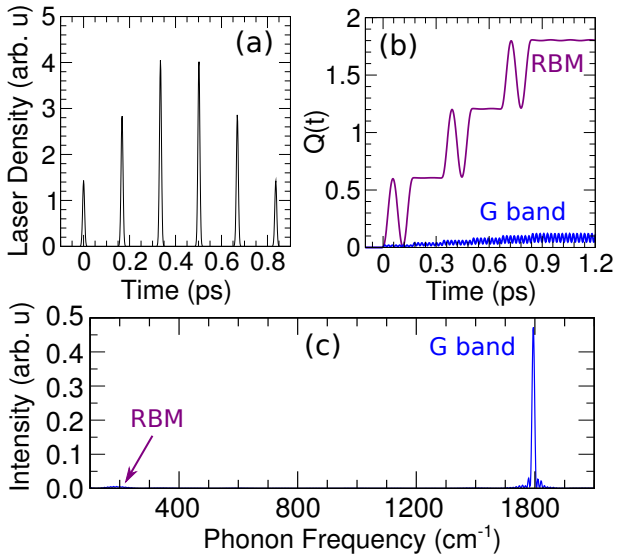

Figure 4. A possible way to suppress the RBM while at the same time keeping the G-band is by using $T_{\rm rep}$ with the value of half-integer multiple of $T_{\rm RBM}$, but τ_p should be less than $T_{\rm G}$. Panel (a) shows the laser density of the pulse train with $T_{\rm rep} = 1.5\ T_{\rm RBM}$, $\tau_p = 10$ fs, and $N_{\rm pulse} = 6$. Panel (b) shows the resulting RBM and G-band oscillation amplitudes. Panel (c) shows the coherent phonon intensity for the RBM and G-band. The intensity is the Fourier transform of the absorption modulation $\Delta\alpha$ due to the coherent phonon oscillations. The RBM in this case almost disappears while the G-band survives.

destructive interference for the RBM. To suppress the RBM while still keeping the G-band, we propose a trick that the repetition period should instead be of half-integer multiple of the RBM period by keeping the same number of pulses (e.g., $N_{\rm pulse} = 6$). Thus, the RBM is completely suppressed because of destructive interference, while the G-band still survives. Another alternative is by still using $T_{\rm rep} = T_{\rm G}$ but increasing the number of pulses. This latter way may be justified by checking the behavior of a certain phonon mode amplitude excited with different number of pulses. For example, in the inset of figure 3 we show RBM phonon amplitudes generated by a single Gaussian pulse (dashed line) and by a pulse (solid line) with the same $\tau_p = 10$ fs (additionally we also have $N_{\rm pulse} = 6$ and $T_{\rm rep} = T_{\rm G} = 20.9$ fs for the pulse train). We can see that using the pulse train with $T_{\rm rep} = T_{\rm G}$ can already reduce the RBM amplitude because the repetition period does not coincide with the integer multiple of $T_{\rm RBM}$.

Now let us see what happens to the RBM and the G-band when $T_{\rm rep}$ is selected to be half-integer multiple of $T_{\rm RBM}$. Figure 4(a) shows the pulse train profile with repetition period $T_{\rm rep} = 1.5\ T_{\rm RBM}$ and pulse width $\tau_p = 10$ fs for $(11, 0)$ SWNT, while figure 4(b) shows the resulting coherent phonon amplitude for the RBM and the G-band. We do not consider yet the decay of the photoexcited cariers (in several ps) for simplicity. It is noted in figure 4(b) that the displacive constant amplitude of $Q(t)$ shifts for every additional pulse. It is reasonable in our approximation because a cancellation of vibration occurs while expansion of bond length takes place by increasing the number of photo-excited carriers. However, the constant value of $Q(t)$ does not contribute to $I(\omega)$ in equation (9) except for $\omega = 0$. It means that applying $\tau_p = 10$ fs warrants the excitation of the G-band, while by applying $T_{\rm rep} = 1.5\ T_{\rm RBM}$ we can filter the RBM. We expect that the origin of this phenomenon is related to the interference effect. The RBM is completely suppressed due to the destructive interference. We further confirm this argument by calculating the coherent phonon intensity of the RBM and the G-band from equations (7)–(9), as shown in figure 4(c). In the experiment of coherent phonon spectroscopy, the coherent phonon intensity is a Fourier transform intensity (power spectrum) from either the differential transmittance or reflectance [6,9]. However, in this work, we calculate the coherent phonon intensity from the absorption modulation $\Delta\alpha$ because ΔT or ΔR is proportional to $\Delta\alpha$. From figure 4(c), we clearly see that the RBM (G-band) could be suppressed (kept) by this technique. It should be noted that some ripples appearing near the main peaks are due to the numerical limitation of our Fourier transform program, which can safely be neglected.

Although we have shown that $T_{\rm rep} = 1.5\ T_{\rm RBM}$ could be used to keep the G-band while suppresing the RBM, this approach might not be handy for experimentalists since they need to ensure their sample only consists of a single SWNT chirality. To overcome this limitation for the bundled sample having a lot of SWNT chiralities mixed inside it, we may employ another approach of pulse-train treatment by utilizing many pulses within the pulse train. In this case, if we want to selectively excite the G-band, it is not necessary to apply $T_{\rm rep} = 1.5\ T_{\rm RBM}$. Instead, we may again use $T_{\rm rep} = T_{\rm G}$ (or integer multiple of the G-band period) by increasing the number of laser pulses.

Figure 5(a) shows an example of the pulse train with 50 Gaussian pulses and 90 Gaussian pulses with $\tau_p = 10$ fs. Figure 5(b) displays the resulting coherent phonon amplitude for the RBM and G-band of the $(11, 0)$ SWNT. We can see that basically the larger the number of pulses is, the smaller the RBM amplitude could be. To confirm this behavior, we calculate the ratio between the peak intensity of the G-band and that of the RBM, denoted by $I_{\rm G}/I_{\rm RBM}$, by varying $N_{\rm pulse}$ within 10–90. We perform the calculation by both numerical and analytical methods and the results are shown in figure 5(c). The numerical results are denoted by filled diamonds in figure 5(c). The numerical calculation was performed for every 10-pulse increment due to the expensive calculation by

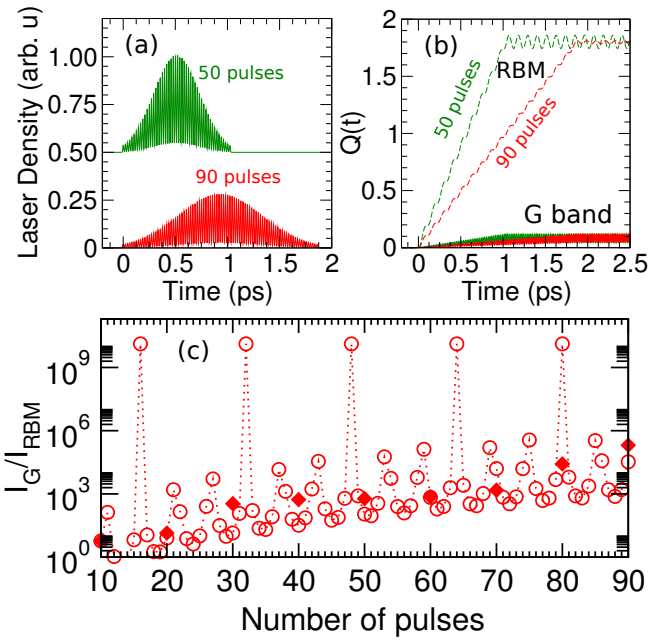

Figure 5. An alternative approach to keep the G-band and suppress the RBM by considering the dependence of coherent phonon intensity on the number of pulses in the pulse train. (a) Laser density profile in the case of 50 and 90 laser pulses. (b) The resulting coherent phonon amplitudes due to the applied pulse train for the RBM (dashed line) and the G-band (solid line), each is shown for the two different number of laser pulses. (c) Ratio between coherent phonon intensity of the G band ($I_{\rm G}$) and the RBM ($I_{\rm RBM}$) versus the number of pulses. The numerical results are denoted by filled diamonds, plotted every 10 pulses due to heavy computational time. The analytical results are denoted by open circles, plotted every 1 pulse and connected with dotted lines as a guide for eyes. Note that for comparing two approaches, the analytical results are normalized to numerical $I_{\rm G}/I_{\rm RBM}$ at $N_{\rm pulse} = 10$. The SWNT chirality considered here is $(11, 0)$ and the pulse repetition rate is $T_{\rm rep} = T_{\rm G}$.

increasing $N_{\rm pulse}$.

We find that as we increase $N_{\rm pulse}$, the value of $I_{\rm G}$ can be much larger than $I_{\rm RBM}$, which indicates a very clear selectivity of the G-band phonon. The reason of the fine selection is that by using larger $N_{\rm pulse}$ with $T_{\rm rep} = T_{\rm G}$, there is a higher possibility to have destructive interference for the RBM. To understand this behavior more clearly, we examine the analytical solution of $A_{\rm max}$ from equation (20) for the G-band ($A_{\rm G}$) and for the RBM ($A_{\rm RBM}$), and then we plot the analytical $I_{\rm G}/I_{\rm RBM}$ by assuming that

$$\frac{I_{\rm G}}{I_{\rm RBM}} \propto \left(\frac{A_{\rm G}}{A_{\rm RBM}}\right)^4. \tag{21}$$

This assumption is justified as follows. We estimate that the coherent phonon amplitude $Q(t)$ (or $A_{\rm max}$) linearly influences the optical matrix element $P_{nn'}(k, t)$ in equation (7) which has a power of two, while the coherent phonon intensity in equation (9) also has another power of two. Therefore, the intensity can be roughly approximated proportional to $A^4_{\rm max}$. By inserting some parameters from the numerical results ($T_{\rm rep}$, $T_{\rm G}$, and $T_{\rm RBM}$) into the analytical formula, we can plot the analytical $I_{\rm G}/I_{\rm RBM}$ for the increase of N_{pulse} every 1 pulse, denoted by open circles in figure 5(c). To compare the two approaches, we also normalize the analytical results to the numerical $I_{\rm G}/I_{\rm RBM}$ at $N_{\rm pulse} = 10$.

It can be seen that the basic trend of the numerical results in figure 5(c) agrees well with the analytical results, i.e., increasing $N_{\rm pulse}$ tends to improve the G-band selectivity. Interestingly, the analytical results in figure 5(c) give us more insight on the other regimes of $N_{\rm pulse}$, in which some sudden increase of $I_{\rm G}/I_{\rm RBM}$ may take place periodically at particular values of $N_{\rm pulse}$. We expect that the origin of this behavior for $T_{\rm rep} = T_{\rm G}$ might be related with the following relation:

$$r_i = \frac{N_{\rm pulse} T_{\rm G}}{T_{\rm RBM}} \approx i, \tag{22}$$

where r_i is a magic ratio and i is a positive integer. For example, we can check that for $T_{\rm G} = 20.9\,$fs and $T_{\rm RBM} = 111.5\,$fs, the values of r_i for $N_{\rm pulse} = 16, 32$, and 48 correspond to integers $i = 3, 6$, and 9, respectively. It means that it is still even possible to use few number of pulses in the pulse train to obtain a good selection of the G-band if we can precisely determine the ratio of the G-band and the RBM periods. Furthermore, we may also increase $T_{\rm rep}$ by using a larger integer multiple of $T_{\rm G}$ to overcome the difficulty in making ultrashort repetition periods on the order of subfemtoseconds. In that case, the value of magic ratio is scaled by the integer multiplier.

We expect that the G-band selection method discussed in this section might be useful if we have many different SWNT chiralities in a bundled sample, in which we can suppress the RBMs of different chiralities and keep the G-band. A remaining difficulty for experimentalists regarding this technique might be on generating large number of pulses in the pulse train [14]. For example, the previous experiment on the RBM selectivity have used Gaussian pulses up to 30–40 pulses [17, 30]. Hopefully more development in pump-probe spectroscopy in the near future can allow us to realize a better pulse train system for the G-band and other phonons selective excitation.

3.3. Effect of carrier relaxation

In the above discussions, we neglected the effect of photoexcited carrier relaxation since we only focused on the RBM and G-band selectivity by considering the pulse train repetition period and number of pulses. Neglecting the carrier relaxation time is safe enough for that purpose because the relaxation time $\tau_r \sim 1$ ps is long enough compared with both the pulse duration and the phonon period so that it would not alter

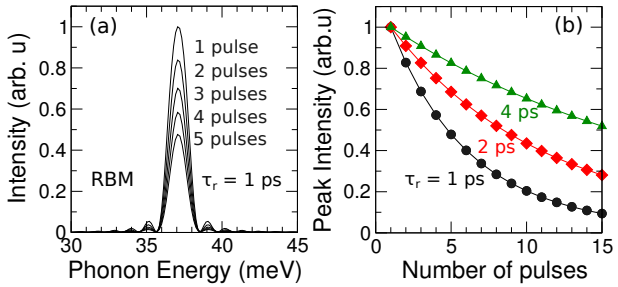

Figure 6. Carrier relaxation effect. (a) Coherent RBM phonon intensity for the (11,0) SWNT calculated by changing the number of pulses. The relaxation time is set to be $\tau_r = 1\,\mathrm{ps}$. (b) Comparison of the coherent RBM phonon intensity for the (11,0) SWNT for different relaxation time: $\tau_r = 1\,\mathrm{ps}$ (circles), $\tau_r = 2\,\mathrm{ps}$ (diamonds), and $\tau_r = 4\,\mathrm{ps}$ (triangles), which fit well with analytical lines. The pulse train repetition period in both panels (a) and (b) is $T_{\mathrm{rep}} = T_{\mathrm{RBM}}$ and the pulse width is $\tau_p = 50\,\mathrm{fs}$. All the intensity values are normalized to unity with respect to the intensity at $N_{\mathrm{pulse}} = 1$.

the conditions of phonon selectivity. However, the photoexcited carrier relaxation can affect the exact amplitude of coherent phonons and hence the coherent phonon intensity, especially when the number of pulses increase, the total pulse duration becomes comparable to τ_r. Here we are particularly interested in how the coherent phonon intensity would evolve by changing the number of pulses in the pulse train when we include the carrier relaxation effects. The relaxation effects are considered through equation (6) and the coherent phonon intensity is recalculated using equations (7)–(9).

In figure 6(a), we show an example of the effects of the carrier relaxation on the coherent phonon intensity, in which the RBM intensity decreases when we increase the number of pulses in the pulse train. In this case, we set the relaxation time $\tau_r = 1\,\mathrm{ps}$, the pulse repetition period $T_{\mathrm{rep}} = T_{\mathrm{RBM}}$, and the pulse width $\tau_p = 50\,\mathrm{fs}$. In figure 6(b), we vary the values of τ_r and plot the peak RBM intensity as a function of number of pulses for $\tau_r = 1\,\mathrm{ps}$, $2\,\mathrm{ps}$, and $4\,\mathrm{ps}$. We also fit the numerical data with equation (17), calculating its A_{max} for the RBM with an assumption that $I_{\mathrm{RBM}} \propto (A_{\mathrm{RBM}})^4$. As the relaxation time increases, a flatter function of peak intensity is obtained as a function of number of pulses following an exponential feature. In the limit of $\tau_r \to \infty$, the peak intensity becomes constant, independent of the number of pulses, since we have assumed that the source laser power is divided into several pulses in the pulse train. We expect that such a behavior could be useful to estimate the carrier relaxation time from experiments if we suppose that τ_r is initially unknown, i.e., experimentalists can try measuring the coherent phonon spectra by changing the number of pulses in the pulse train and observe the exponential decrease of the peak intensity versus number of pulses.

4. Conclusion

We have obtained some conditions for the pulse-train technique to excite a specific coherent phonon mode in SWNTs while suppressing the other phonon modes. As the basic condition, it is necessary to use the laser pulse width shorter than a typical phonon period for such a phonon mode to be excited. Then, for the RBM, the mode selection can be achieved if the pulse repetition period matches with integer multiple of the phonon period. In the case of the G-band, the repetition period should be of half-integer multiple of the RBM phonon period or of integer multiple of the G-band period with a large number of pulses giving a certain value of magic ratio. From this simulation, we expect that the pulse-train technique can be generally used for selectively exciting a specific phonon mode in other materials, which might be useful for optomechanical applications or for developing phononic devices.

Acknowledgments

We are grateful to Prof. C. J. Stanton, Prof. J. Kono, Dr. J.-H. Kim, and Dr. G. D. Sanders (University of Florida, USA) for our previous collaborations which stimulated the present work and for their sharing the coherent phonon simulation code which we have developed further in our group. A.R.T.N. acknowledges the Interdepartmental Doctoral Degree Program for Material Science Leaders at Tohoku University for providing a financial support. R.S. and E.H.H. acknowledge JSPS KAKENHI Grant Nos. JP25286005 and JP225107005.

References

[1] Dumitrică T, Garcia M E, Jeschke H O and Yakobson B I 2004 *Phys. Rev. Lett.* **92** 117401
[2] Gambetta A, Manzoni C, Menna E, Meneghetti M, Cerullo G, Lanzani G, Tretiak S, Piryatinski A, Saxena A, Martin R L and Bishop A R 2006 *Nat. Phys.* **2** 515–520
[3] Lim Y S, Yee K J, Kim J H, Haroz E H, Shaver J, Kono J, Doorn S K, Hauge R H and Smalley R E 2006 *Nano Lett.* **6** 2696–2700
[4] Lüer L, Gadermaier C, Crochet J, Hertel T, Brida D and Lanzani G 2009 *Phys. Rev. Lett.* **102** 127401
[5] Makino K, Hirano A, Shiraki K, Maeda Y and Hase M 2009 *Phys. Rev. B* **80** 245428
[6] Zeiger H J, Vidal J, Cheng T K, Ippen E P, Dresselhaus G and Dresselhaus M S 1992 *Phys. Rev. B* **45** 768–778
[7] Kuznetsov A V and Stanton C J 1994 *Phys. Rev. Lett.* **73** 3243–3246
[8] Hu X and Nori F 1996 *Phys. Rev. B* **53** 2419–2424
[9] Merlin R 1997 *Solid State Commun.* **102** 207–220
[10] Lim Y S, Nugraha A R T, Cho S J, Noh M Y, Yoon E J, Liu H, Kim J H, Telg H, Hroz E H, Sanders G D, Baik S H, Kataura H, Doorn S K, Stanton C J, Saito R, Kono J and Joo T 2014 *Nano Lett.* **14** 1426–1432
[11] Eichler A, Moser J, Chaste J, Zdrojek M, Wilson-Rae I and Bachtold A 2011 *Nat. Nanotechnol.* **6** 339–342
[12] Ruskov R and Tahan C 2012 *JPCS* **398** 012011

[13] Li J J and Zhu K D 2012 *Sci. Rep.* **2** 903
[14] Weiner A M, Leaird D E, Wiederrecht G P and Nelson K A 1990 *Science* **247** 1317
[15] Hase M, Itano T, Mizoguchi K and Nakashima S i 1998 *Jpn. J. Appl. Phys.* **37** L281
[16] Watanabe K, Takagi N and Matsumoto Y 2005 *Phys. Chem. Chem. Phys.* **7** 2697
[17] Kim J H, Han K J, Kim N J, Yee K J, Lim Y S, Sanders G D, Stanton C J, Booshehri L G, Hároz E H and Kono J 2009 *Phys. Rev. Lett.* **102** 037402
[18] Saito R, Dresselhaus G and Dresselhaus M S 1998 *Physical Properties of Carbon Nanotubes* (London: Imperial College Press)
[19] Dresselhaus M S, Dresselhaus G, Saito R and Jorio A 2005 *Phys. Rep.* **409** 47–99
[20] Sanders G D, Nugraha A R T, Sato K, Kim J H, Kono J, Saito R and Stanton C J 2013 *J. Phys. Condens. Mattter* **25** 144201
[21] Kim J H, Nugraha A R T, Booshehri L G, Haroz E H, Sato K, Sanders G D, Yee K J, Lim Y S, Stanton C J, Saito R and Kono J 2013 *Chem. Phys.* **413** 55–80 ISSN 0301-0104
[22] Popov V N and Henrard L 2004 *Phys. Rev. B* **70** 115407
[23] Jiang J, Saito R, Samsonidze G G, Chou S G, Jorio A, Dresselhaus G and Dresselhaus M S 2005 *Phys. Rev. B* **72** 235408
[24] Kim J H, Yee K J, Lim Y S, Booshehri L G, Hároz E H and Kono J 2012 *Phys. Rev. B* **86**(16) 161415
[25] Chuang S L 1995 *Physics of optoelectronic devices* (New York: Wiley)
[26] Grüneis A, Saito R, Samsonidze G G, Kimura T, Pimenta M A, Jorio A, Filho A G S, Dresselhaus G and Dresselhaus M S 2003 *Phys. Rev. B* **67** 165402
[27] Nugraha A R T, Hasdeo E H, Sanders G D, Stanton C J and Saito R 2015 *Phys. Rev. B* **91** 045406
[28] Ichida M, Hamanaka Y, Kataura H, Achiba Y and Nakamura A 2002 *Physica B* **323** 237–238
[29] Lauret J S, Voisin C, Cassabois G, Delalande C, Roussignol P, Jost O and Capes L 2003 *Phys. Rev. Lett.* **90** 057404
[30] Sanders G D, Stanton C J, Kim J H, Yee K J, Lim Y S, Hároz E H, Booshehri L G, Kono J and Saito R 2009 *Phys. Rev. B* **79** 205434